Kazuya Yoshida

Department of Aeronautics and Space Engineering
Tohoku University
Sendai, 980-8579, Japan
yoshida@astro.mech.tohoku.ac.jp

Engineering Test Satellite VII Flight Experiments For Space Robot Dynamics and Control: Theories on Laboratory Test Beds Ten Years Ago, Now in Orbit

Abstract

The Engineering Test Satellite VII (ETS-VII), an unmanned spacecraft equipped with a 2-m long, six-degree-of-freedom manipulator arm, was developed and launched by the National Space Development Agency of Japan (NASDA). ETS-VII has successfully carried out a variety of on-board experiments with its manipulator arm, and these key technologies are essential for an orbital free-flying robot. These results will provide a solid basis for future satellite servicing missions. This paper highlights manipulator control utilizing the concepts of the generalized Jacobian matrix and the reaction null-space. These concepts have been proposed and discussed for the past ten years using laboratory test beds, and their practical application has now been demonstrated in orbit.

KEY WORDS—space manipulator, reaction dynamics, satellite servicing

1. Introduction

The possibility of a free-flying space robot rescuing and servicing malfunctioning satellites has been discussed since the early 1980s (for example, Akin et al. 1983), but very few experiments have ever been attempted in orbit. The maintenance missions for the Hubble Space Telescope and the retrieval of the Space Flyer Unit (Ohkami and Oda 1999) are two such examples that were carried out with the Space Shuttle Remote Manipulator System. However, in these missions the flight crews manually operated the manipulator arm. Autonomous target capture by an unmanned space robot, on the other hand, has long been considered a challenge within the space robotics community.

The Robot Technology Experiment, ROTEX, developed by the German Aerospace Center (DLR), was one of the important milestones of robot technology in space (Hirzinger et al. 1993). A multisensory robot was flown on space shuttle COLUMBIA (STS-55) in 1993. Although the robot worked inside a work cell on the shuttle, several key technologies such as a multisensory gripper, teleoperation from the ground, shared autonomy, and time-delay compensation by a predictive graphic display were successfully tested.

The Engineering Test Satellite VII (ETS-VII, Figure 1) is another milestone in the development of robot technology in space, particularly in the area of satellite servicing. ETS-VII is an unmanned spacecraft developed and launched by the National Space Development Agency of Japan (NASDA) in November 1997. It successfully completed a series of experiments with a 2-m long, six-degrees-of-freedom (6-DOF) manipulator arm mounted on its exterior. The mission objective of ETS-VII was to test existing robotics technology and to demonstrate its utility in unmanned orbital operation and servicing tasks. The mission consisted of two subtasks: autonomous rendezvous/docking (RVD) and a number of robot experiments (RBT). The robot experiments included: (1) teleoperation from the ground with a large time delay; (2) robotic servicing task demonstrations such as ORU exchange and deployment of a space structure; (3) dynamically coordinated control between the manipulator's reaction and the satellite's

The International Journal of Robotics Research
Vol. 22, No. 5, May 2003, pp. 321-335,

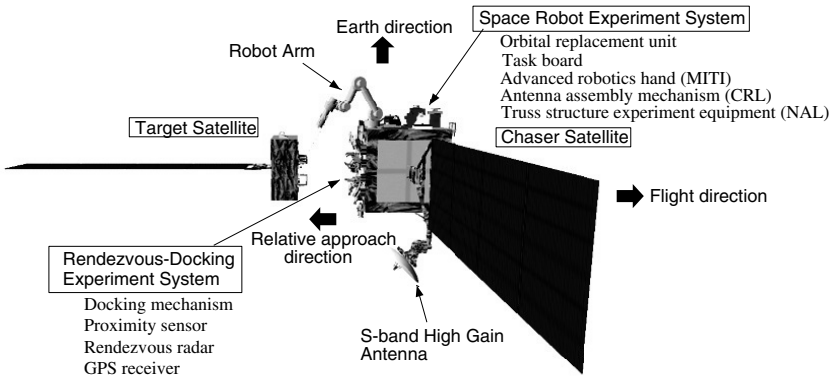

Fig. 1. The Engineering Test Satellite VII.

response; and (4) capture and berthing of a target satellite. Early reports on some of these experiments have been made in previous papers (Ohkami and Oda 1999; Oda et al. 1996; Kasai, Oda, and Suzuki 1999).

These planned flight experiments were successfully completed by the end of May 1999. Since the spacecraft was still operational and in good condition, however, the mission period was extended until the end of December. In this period, academic proposals were collected and research groups from universities were given the opportunity to conduct flight experiments. The author was given the chance to carry out experiments that highlighted the motion dynamics of a free-flying space robot, thereby verifying the theories on coupling and coordination between the manipulator and the base spacecraft. Early reports on this experiment have been made in previous publications (Yoshida 1999; Yoshida et al. 2000a, b).

A free-flying space robot, including the ETS-VII, is characterized by its reaction dynamics. Due to the manipulator's motion, the position and orientation of the base spacecraft receives an undesirable disturbance that could degrade the performance of the robot operation. The disturbance forces can be understood as a simple reaction-to-action, but in order to understand the motion of the system subject to the reaction and to prescribe a proper control, complicated issues involving angular momentum must first be tackled. Numerous studies concerning these reaction dynamics issues have been conducted by a number of researchers (Vafa and Dubowsky 1987, 1990; Umetani and Yoshida 1987, 1989a; Dubowsky and Torres 1990, 1991; Yoshida, Nenchev, and Uchiyama 1996; Nenchev et al. 1999; Yoshida 1994; Oda 1996; Nakamura and Mukherjee 1991; Rui, Kolmanovsky, and McClamroch 1998; Xu and Kanade 1993).

Some earlier concepts such as the virtual manipulator (Vafa and Dubowsky 1987, 1990) and the generalized Jacobian matrix (GJM; Umetani and Yoshida 1987, 1989a) are useful in modeling the coupled motion of the arm and the base, allowing for improved control under the induced reaction forces. Other methods have been developed to improve the motion planning in order to have a minimum disturbance on the base (Dubowsky and Torres 1990, 1991). These methods represent the degrees of coupling on a disturbance map, and then a course of optimum manipulation can be charted. A set of solutions called the reaction null-space (RNS; Yoshida, Nenchev, and Uchiyama 1996; Nenchev et al. 1999) has been derived to chart the case of minimum disturbance. The manipulator motion belonging to this space is decoupled from the reaction, thereby yielding zero disturbance on the base. Manipulator operation of this type is referred to as a *reactionless* manipulation. If the base motion controller were able to anticipate a disturbance, a feed-forward signal could be produced to improve the recovery performance of the base (Yoshida 1994). *Coordinated* reaction control is the method by which the feed-forward compensation of the anticipated disturbance is generated (Oda 1996).

The angular momentum equation plays an important role in describing the relationship between the manipulator motion and the base reaction, but has complicated non-linear characteristics called *non-holonomic* characteristics. For example, through the repetition of a cyclic motion, a manipulator arm can substantially change a spacecraft's orientation (Vafa and Dubowsky 1990). The non-holonomic characteristic of these motions requires the expertise of the non-linear mechanics community to be applied to the area of motion planning and non-linear control. There are currently a number of papers published concerning this area of research, for example Nakamura and Mukherjee (1991) and Rui, Kolmanovsky, and McClamroch (1998).

In the robotics flight experiments on ETS-VII, several of the above motion control theories have been tested and verified. This paper focuses on the GJM and the RNS concepts, in

particular. These concepts have been explored using laboratory test beds for the past ten years, and their future viability in missions is now conceivable due to the successful orbital demonstration by the ETS-VII.

This paper is organized as follows. In Section 2, the motion dynamics characterizing a free-flying space robot and the derivation of key concepts, including the GJM and RNS, are explained. Section 3 reviews the experimental verifications of these concepts on laboratory test beds, which were conducted prior to the ETS-VII mission. In Section 4, the orbital data from the 1999 ETS-VII flight experiments are described. Finally, the viability of future target capture operations is discussed in Section 5. This discussion includes complementary simulations of the target capture operation.

2. Dynamics of a Free-Flying Space Robot

A free-flying space robot can be uniquely characterized by its motion dynamics. The motion of the manipulator arm induces a reaction motion on its base, and the motion of the entire system is subject to the principle of momentum conservation. This reaction can also be regarded as a disturbance upon the base of the satellite. Hence, the coupling and the coordination between the arm and the base become an important issue for the successful operation of the system. This is the main difference from a terrestrially based robot manipulator, and it becomes a major concern when controlling one in space. Early papers on the modeling and control of a free-flying robot can be found in Xu and Kanade (1993). In this section, we review basic modeling techniques, focusing on two key concepts: the GJM and the reactionless manipulation.

2.1. Basic Equations

The equation of motion for a free-flying space robot that equips an n-DOF manipulator arm is described by

$$\begin{bmatrix} \mathbf{H}_b & \mathbf{H}_{bm} \\ \mathbf{H}_{bm}^{\mathrm{T}} & \mathbf{H}_m \end{bmatrix} \begin{bmatrix} \ddot{\mathbf{x}}_b \\ \ddot{\boldsymbol{\phi}} \end{bmatrix} + \begin{bmatrix} \mathbf{c}_b \\ \mathbf{c}_m \end{bmatrix} = \begin{bmatrix} \mathcal{F}_b \\ \boldsymbol{\tau} \end{bmatrix} + \begin{bmatrix} \mathbf{J}_b^{\mathrm{T}} \\ \mathbf{J}_m^{\mathrm{T}} \end{bmatrix} \mathcal{F}_h, \tag{1}$$

where $\dot{\mathbf{x}}_b = (\mathbf{v}_b^{\mathrm{T}}, \boldsymbol{\omega}_b^{\mathrm{T}})^{\mathrm{T}} \in R^6$ denotes the linear and angular velocity of the base satellite (reference body) and $\dot{\boldsymbol{\phi}} \in R^n$ denotes the motion rate of the manipulator joints. Other symbols are defined as follows:

$\mathbf{H}_b \in R^{6\times 6}$ = inertia matrix of the base;

$\mathbf{H}_m \in R^{n\times n}$ = inertia matrix of the manipulator arm;

$\mathbf{H}_{bm} \in R^{6\times n}$ = coupling inertia matrix;

$\mathbf{c}_b \in R^6$ = velocity-dependent non-linear term of the base;

$\mathbf{c}_m \in R^n$ = velocity-dependent non-linear term of the manipulator arm;

$\mathcal{F}_b \in R^6$ = force and moment exert on the centroid of the base;

$\mathcal{F}_h \in R^6$ = force and moment exert on the manipulator hand;

$\boldsymbol{\tau} \in R^n$ = manipulator joint torque;

$\mathbf{J}_b \in R^{6\times 6}$ = Jacobian matrix for the base;

$\mathbf{J}_m \in R^{6\times n}$ = Jacobian matrix for the manipulator arm.

When a system is freely floating in space, such as in this case, the *external* wrenches on the base and the manipulator hand are assumed to be zero; i.e., $\mathcal{F}_b = \mathbf{0}$, $\mathcal{F}_h = \mathbf{0}$, respectively. The motion of the robot is governed only by the *internal* torque of the manipulator joints $\boldsymbol{\tau}$, and hence the linear and angular momenta of the system $(\mathcal{P}^{\mathrm{T}}, \mathcal{L}^{\mathrm{T}})^{\mathrm{T}} \in R^6$ remain constant.

$$\begin{bmatrix} \mathcal{P} \\ \mathcal{L} \end{bmatrix} = \mathbf{H}_b \dot{\mathbf{x}}_b + \mathbf{H}_{bm} \dot{\boldsymbol{\phi}}. \tag{2}$$

2.2. Angular Momentum

The integral of the upper set of eq. (1) gives a momentum equation, as shown in eq. (2), which is composed of the linear and angular momenta. When the linear momentum is further integrated, the result verifies the principle that the mass centroid of the entire system either remains stationary or translates with a constant velocity.

The angular momentum equation, however, does not have a second integral, and therefore provides a first-order nonholonomic constraint. The equation can be expressed as follows

$$\tilde{\mathbf{H}}_b \boldsymbol{\omega}_b + \tilde{\mathbf{H}}_{bm} \dot{\boldsymbol{\phi}} = \mathcal{L}, \tag{3}$$

where $\mathcal{L}$ is the initial angular momentum, and the inertia matrices with a tilde ($\tilde{\cdot}$) are those modified from eq. (2) (Xu and Kanade 1993). $\tilde{\mathbf{H}}_{bm}\dot{\boldsymbol{\phi}}$ represents the angular momentum generated by the manipulator motion.

Equations (3) can be solved for $\boldsymbol{\omega}_b$ with zero initial angular momentum:

$$\boldsymbol{\omega}_b = -\tilde{\mathbf{H}}_b^{-1} \tilde{\mathbf{H}}_{bm} \dot{\boldsymbol{\phi}}. \tag{4}$$

This expression describes the resulting disturbance motion of the base when there is joint motion in the manipulator arm.

It should be noted that the disturbance map approach uses this equation. The magnitudes and directions of maximum and minimum disturbance can be obtained from the singular value decomposition of the matrix $\left[-\tilde{\mathbf{H}}_b^{-1}\tilde{\mathbf{H}}_{bm}\right]$, and displayed on the map (Dubowsky and Torres 1990, 1991). Equation (4) is also used for the feed-forward compensation in the coordinated manipulator/base control model (Yoshida 1994; Oda 1996).

2.3. Generalized Jacobian Matrix

The velocity of the manipulator hand in the inertial frame is expressed as

$$^{(i)}\dot{\mathbf{x}}_h = \mathbf{J}_m\dot{\boldsymbol{\phi}} + \mathbf{J}_b\dot{\mathbf{x}}_b, \tag{5}$$

where the superscript i indicates that the vector is described with respect to the inertia frame.

Combining this equation and eq. (2) yields an equation directly relating the joint rate and hand velocity of the manipulator arm. This is accomplished by canceling out the base variables.

$$^{(i)}\dot{\mathbf{x}}_h = \mathbf{J}_g\dot{\boldsymbol{\phi}} \tag{6}$$

$$\mathbf{J}_g = \mathbf{J}_m - \mathbf{J}_b\mathbf{H}_b^{-1}\mathbf{H}_{bm}, \tag{7}$$

where $(\mathcal{P}^{\mathrm{T}}, \mathcal{L}^{\mathrm{T}})^{\mathrm{T}} = \mathbf{0}$ has been assumed for simplification. The matrix $\mathbf{J}_g$ is called the GJM (Umetani and Yoshida 1987, 1989a). Using this matrix, the manipulator hand can be operated under a resolved motion-rate control or resolved acceleration control in the inertial space, and while it allows for a base reaction, the hand is not disturbed by it.

2.4. Reaction Null-Space

From a practical point of view, any change in the attitude is not desirable. This is the reason why manipulator motion planning methods that minimize the base attitude disturbance have been one of research focuses. Indeed, the ultimate goal of achieving zero disturbance is possible. This becomes apparent from analyzing the angular momentum equation.

The following is the angular momentum equation with zero initial angular momentum $\mathcal{L} = \mathbf{0}$ and zero attitude disturbance $\boldsymbol{\omega}_b = \mathbf{0}$:

$$\tilde{\mathbf{H}}_{bm}\dot{\boldsymbol{\phi}} = \mathbf{0}. \tag{8}$$

This equation yields the following null-space solution:

$$\dot{\boldsymbol{\phi}} = (\mathbf{I} - \tilde{\mathbf{H}}_{bm}^{+}\tilde{\mathbf{H}}_{bm})\dot{\boldsymbol{\zeta}}. \tag{9}$$

The joint motion given by this equation is guaranteed to not disturb the base attitude. Here the vector $\dot{\boldsymbol{\zeta}} \in R^n$ is arbitrary and the null-space of the inertia matrix $\tilde{\mathbf{H}}_{bm} \in R^{3\times n}$ is called RNS (Yoshida, Nenchev, and Uchiyama 1996).

The DOF for $\dot{\boldsymbol{\zeta}}$ is $n - 3$, and the manipulator arm on the ETS-VII has six DOF, i.e., $n = 6$. Therefore, there remain three DOF in the RNS. These DOF can be specified by introducing additional criteria. In the flight experiment presented later, the zero reaction on the base is realized by constraining the orientation of the manipulator hand (three DOF) while allowing for the translation of the hand (three DOF). This manipulator motion is called reactionless manipulation (Nenchev et al. 1999).

2.5. Cases with Non-Zero Momentum

Here, a note should be made for the cases of a non-zero system momentum. Increment or decrement of the system momentum occurs when the system is under the effect of external forces generated by attitude control devices such as gas jet thrusters, or natural forces such as the interaction with the geomagnetism, or the gradient of gravity.

In the presence of non-zero system momentum, eq. (6) is modified with an offset velocity, but the definition of the GJM is kept the same as eq. (7):

$$^{(i)}\dot{\mathbf{x}}_h = \mathbf{J}_g\dot{\boldsymbol{\phi}} + \mathbf{J}_b\mathbf{H}_b^{-1}\begin{bmatrix} \mathcal{P} \\ \mathcal{L} \end{bmatrix}.$$

Regarding the RNS model, even with a non-zero $\mathcal{L}$, the manipulator motion given by eq. (9) produces zero momentum and makes any increment or decrement on the existing $\mathcal{L}$. In this sense, this manipulation is understood to be *reactionless.*

Finally, when reaction wheels are mounted on the base spacecraft, angular momentum is accumulated in the wheels when the base attitude is maintained against the external forces. Or, in case with bias-momentum wheels, the system always has non-zero momentum in the base. In these cases, eq. (1) should be augmented with the motion of wheels using their rotational velocity as an additional generalized coordinate. By this augmentation, the gyroscopic effect of the wheels is also taken into account. Or, alternatively, the gyroscopic effect $\boldsymbol{\omega}_b \times \mathcal{L}$ can be directly put in $\mathcal{F}_b$ considering it as an external force.

2.6. Gravity Gradient Torque

Gravity gradient torque is one of the common sources of attitude disturbance on a spacecraft in orbit. In the modeling and control of a space robot, however, this effect has been neglected because the disturbance from the manipulator reaction is dominant for a short time-range compared to an orbital period. After looking at the flight data for the ETS-VII, though, the gravity gradient torque cannot be neglected even in the short-range. It should particularly not be neglected when the spacecraft is in a free-floating situation and the attitude control devices are turned off. This situation results in *free-drift* motion.

The gravity gradient torque $\mathbf{N}$ is the result of the gravitational force varying over the length of the spacecraft (Hughes 1986). This torque can be modeled by the following equation:

$$\mathbf{N} = \frac{3\mu}{R^5}\mathbf{r} \times \mathbf{I}_{tot}\mathbf{r}. \tag{10}$$

When a space robot is controlled to keep an Earth-facing orientation, like the ETS-VII, the vector $\mathbf{r}$ becomes

$$\mathbf{r} = R\,[\,0\;0\;1\,]^{\mathrm{T}}, \tag{11}$$

where R is a distance between the center of gravity of the Earth and the spacecraft, μ is a gravity constant, and $\mathbf{I}_{tot}$ is the moment of inertia of the entire spacecraft around its centroid.

When the spacecraft is in free-drift, its attitude drifts around an equilibrium point, and when the attitude is controlled by reaction wheels, the disturbance torque $\mathbf{N}$ is accumulated in the wheels as $\Delta\mathcal{L}$:

$$\Delta\mathcal{L} = \mathbf{N}\Delta t. \tag{12}$$

3. Study with Laboratory Test Beds

Laboratory experiments and hardware verification are necessary for the progress of robotics research, but it is difficult to simulate the micro-gravity environment of space in a hardware test bed. There are several methods for conducting laboratory experiments in the area of space robotics. These methods are summarized in the following options: (a) the use of air cushions or other structural supports providing gravity-free motion in the horizontal plane; (b) a tether suspension system that cancels out the gravity (Fujii, Yoneyama, and Uchiyama 1993); (c) neutralizing buoyancy in a water pool; (d) a parabolic flight or a drop-shaft facility; and (e) a hardware-in-the-loop, or *hybrid* simulator (Shimoji et al. 1989; Dubowsky et al. 1994). This paper focuses on option (a), and typical results are reviewed.

3.1. Test Beds for a Free-Flying/Floating Robot

Air-cushion test beds are a frequently used apparatus to simulate the planar motion of a robotic system in the micro-gravity environment. Such test beds have been used in the hardware verification of the Space Shuttle Remote Manipulator System (SRMS; Wargner-Bertak, Middleton, and Hunter 1980), in the Space Station Remote Manipulator System (SSRMS), and in the other manipulator systems that will be mounted on the International Space Station (Morimoto et al. 2002).

Among academic laboratories, Stanford University was one of the first to have performed an extensive study on a flexible manipulator and a free-flying/floating space robot using an air-cushion test bed (Alexander and Cannon 1987; Koningstein, Ullman, and Cannon 1989; Alder and Rock 1994). Tokyo Institute of Technology (TIT) has developed the same type of test bed. The TIT's test bed is called the Experimental Free-Floating Robot Satellite Simulator (EFFORTS; Umetani and Yoshida 1989b; Yoshida 1995).

Figure 2(a) shows a picture of the EFFORTS test bed with a robot model floating using pressurized air on a horizontal glass plate. The test bed was useful in the study of the reaction dynamics of an articulated link system, even though the motion was constrained on a plane. In particular, the manipulation that uses the GJM-based control to reach a floating target has been experimentally verified. The results clearly show that the manipulator end-point properly reaches the target, although the robot base rotated considerably due to the manipulator reaction (see Figure 2(b), and also Extension 1). In order to achieve online target capture control in the experiments, visual servo-tracking was also tested with the real-time measurement of the error between the manipulator hand and the target.

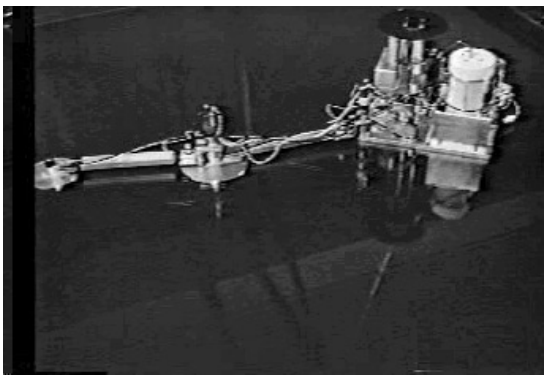

(a)

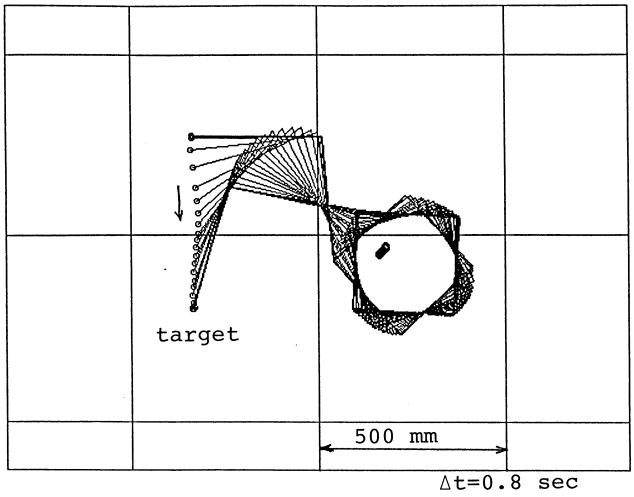

(b)

Fig. 2. A laboratory test bed for a free-flying/floating space robot. (a) The experimental free-floating robot simulator, EFFORTS (1987). (b) A result of target capture experiments by the EFFORTS.

3.2. Test Beds for a Flexible Structure Mounted Robot

A test bed called *Shaky* was developed at the Massachusetts Institute of Technology (MIT) for the study of dynamic coupling between a manipulator arm and its footing base. In the Shaky, a horizontal planar arm is mounted at the end of a flexible beam. The beam produces vibrations in the horizontal plane due to the reaction from the arm. This test bed was used to verify the control algorithms for the end-point control of

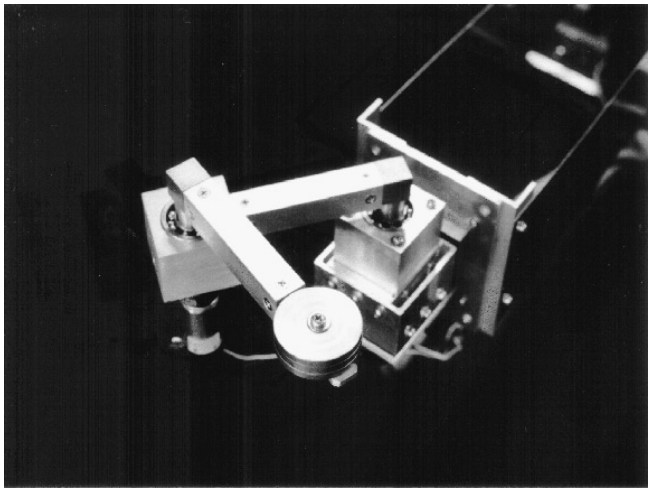

Fig. 3. A laboratory test bed for a flexible-base manipulator system, TREP (1996).

a long reach manipulator (Mavroidis, Rowe, and Dubowsky 1995; Mavroidis, Dubowsky, and Thomas 1996).

Following the Shaky, a similar test bed was constructed at Tohoku University, called *TREP*. Figure 3 shows a picture of the TREP. Using this test bed, the manipulation that does not excite base vibrations as well as effective vibration suppression control were tested. Both control algorithms, which were derived from the RNS, have been verified (Nenchev et al. 1997; Yoshida et al. 1997). Figure 4 shows one of the verification results. The manipulator motion and the resulting vibrations of the base are depicted in Figure 4(a) for the case with a conventional PTP control of the arm. Figure 4(b) shows the results for the case utilizing the RNS-based reactionless manipulation control strategy. See also Extension 2.

4. ETS-VII Flight Experiments

The robotic flight experiment proposed by the author was carried out on September 30, 1999, using three successive flight passes. High-bandwidth communication from/to Tsukuba Space Center, NASDA was possible when ETS-VII was passing through the area of the communication service provided by TDRS, a US data relay satellite located in a geosynchronous orbit above the Pacific ocean. Almost 20 minutes of operation (command uplink) and high-bandwidth telemetry (including video downlink) were conducted in a single flight pass.

The purpose of the flight experiments with a real space system is to prove the theories and algorithms, and to demonstrate their practical viability in the real world. The difficulty, however, is that practical systems always have constraints and restrictions from the system's design specification and safety requirements. For example, the manipulator arm mounted on ETS-VII is a 6-DOF non-redundant arm. The six DOF is a physical constraint. If it was a redundant one, more advanced operation could be explored. An example of a safety constraint is that the existing control system could not be rearranged or re-programed for our experiments. Safety verification of a new software system could take months or years using a ground-based backup model identical to the system in orbit, so the existing system had to be used for these experiments.

Therefore, attempts were made to find ways to maximize this flight opportunity by utilizing a simpler interface with NASDA and by causing a minimum impact on the orbital system. We then planned experiments to demonstrate the basic performance of the proposed concepts and algorithms. These experiments neither commanded the manipulator to make physical contact with other on-board components, nor made any changes to the existing on-board control system. Yet, the ETS-VII had enough system capability to meet the goal of obtaining the essential data for the verification of GJM and RNS concepts, as well as the others.

For the proposed experiment, the manipulator motion trajectories were carefully prepared in the form of motion data sets and the safety of the experiment was preliminarily checked on a NASDA offline simulator. During the experiment, the data sets were uploaded to ETS-VII at a 4 Hz frequency as an isochronous (synchronized) motion command, and the manipulator arm followed the commands in the prepared motion profile.

Figure 5 depicts a detailed configuration of the manipulator arm mounted on ETS-VII. Table 1 shows the kinematic and inertial parameters of the spacecraft and the arm. These inertial parameters were identified before the experiments from the flight telemetry data obtained by NASDA (Yoshida and Abiko 2002). Figure 6 shows a picture obtained from a camera mounted at the shoulder of the arm. It shows on-board components in the foreground and the Earth in the background. Motion pictures obtained by the shoulder and hand cameras are presented in Extension 3, along with the motion of the NASDA real-time simulator. All of these were displayed on the monitors at the robot commander's console during the operation.

4.1. GJM-Based Inertial Manipulation

The GJM-based inertial manipulation experiment was carried out in the free-floating environment without any base attitude control actions and with a zero initial momentum in the system.

Figure 7 illustrates the motion of the arm in the GJM-based manipulation experiment. Because there was no real target floating in the inertial space, a virtual target (depicted by dashed lines in the figure) was simulated in the direction of the Earth's limb. In this experiment the manipulator hand moved 200 mm at 10 mm s^{-1} toward the virtual target while keeping a constant orientation of -22.8 degrees of pitch in the

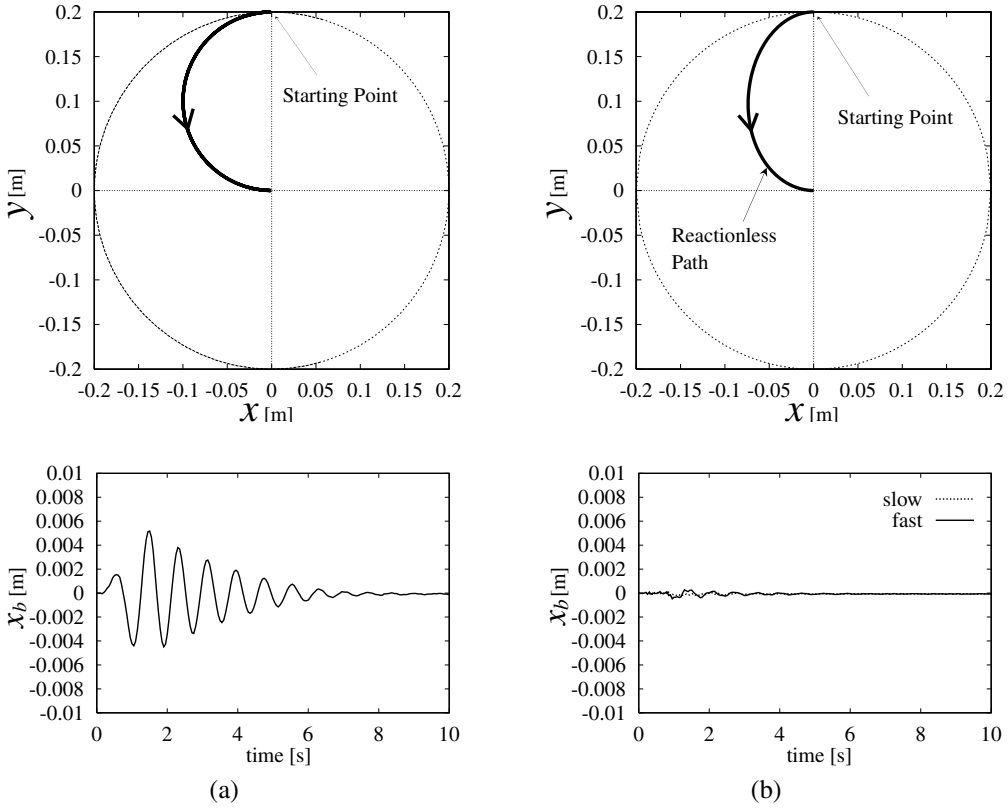

Fig. 4. A comparison of the conventional manipulation and the reactionless manipulation: top, the motion trace of the hand in the Cartesian space; bottom, the vibrations in the flexible base; (a) conventional manipulation; (b) reactionless manipulation.

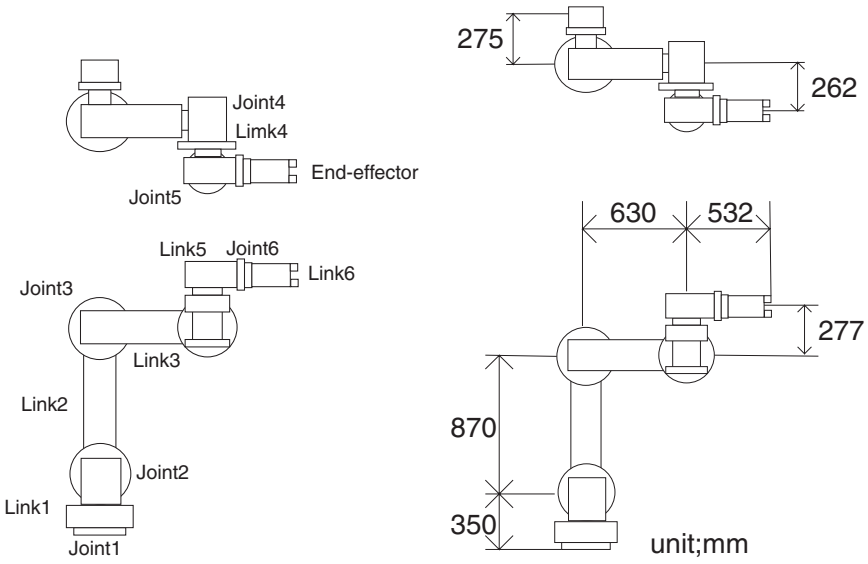

Fig. 5. Kinematic configuration of the manipulator arm mounted on the ETS-VII.

Table 1. Kinematic and Inertial Parameters of ETS-VII

Dimensions of the Arm						
(m)	1	2	3	4	5	6
Link length	0.35	0.87	0.63	0	0	0.53*
Offset	0.28	0	0	0.26	0.28	0
Inertia of the Base						
(kg)	(kgm^2)					
m	I_{xx}	I_{yy}	I_{zz}	I_{xy}	I_{xz}	I_{yz}
2550	6200	3540	7090	48.2	78.5	-29.2
Inertia of the Arm						
Link no	1	2	3	4	5	6
m	35.0	22.5	21.9	16.5	26.0	18.5
I_{zz}	1.69	3.75	2.53	0.072	0.13	0.26

* Link 6 includes a standard end-effector.
** Attachment point of the arm = (−0.79, −0.29, 1.00) m in the satellite base frame.

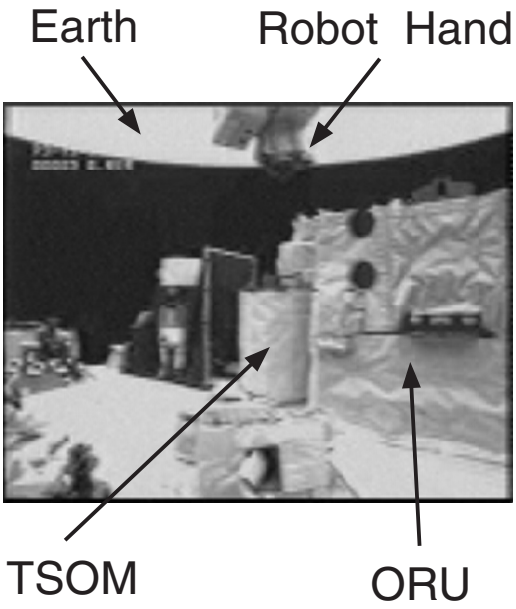

Fig. 6. A video image obtained by an on-board shoulder camera.

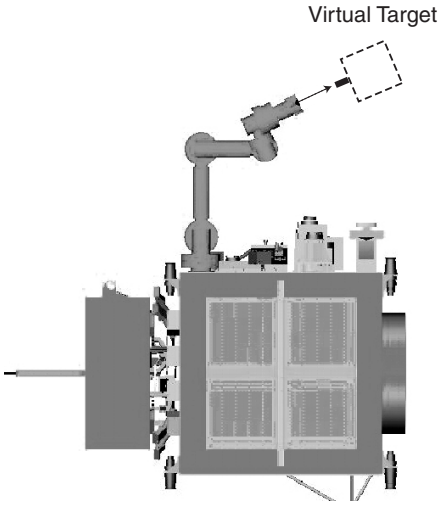

Fig. 7. Experiment for the GJM-based inertial manipulation with a virtual target.

inertial coordinate frame. In this orientation, the hand pointed in the direction of the Earth's limb.

Figure 8 depicts the flight data for the GJM-based manipulation. The motion demonstrated in the figure is a straight-line path tracking in the inertial frame. This motion was regulated by the resolved motion-rate control with the generalized Jacobian using the inversion of eq. (6). Figure 8(a) shows a profile of the pitch angle of the base spacecraft, which rotated by 0.6 degrees due to the reaction moment from the manipulator. Figure 8(b) shows the pitch angle of the manipulator hand with respect to the inertial frame. Using the GJM as the means of the control, the orientation of the hand in the inertial frame is kept at −22.8 degrees during the manipulation (t = 680–770 s), with only very small errors. This is enhanced in Figure 8(c) by displaying the error in the yaw direction on the horizontal axis and the error in the pitch on the vertical axis. The graph corresponds to the view of the hand camera that focused on the (virtual) target during the approach.[1]

The performance of the GJM-based manipulation was then compared with conventional manipulation, i.e., the hand is

1. In this experiment the error in position is not discussed, because there was no way to measure the distance between the hand and the virtual target.

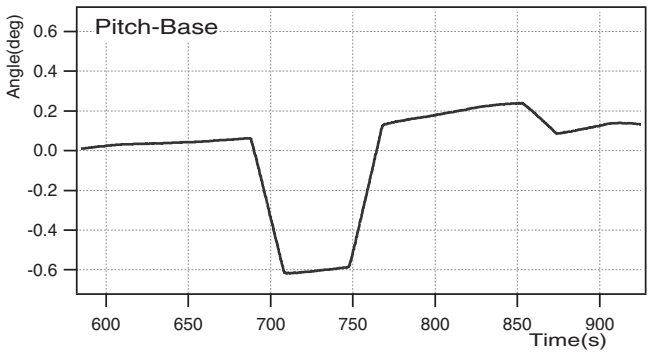

(a)

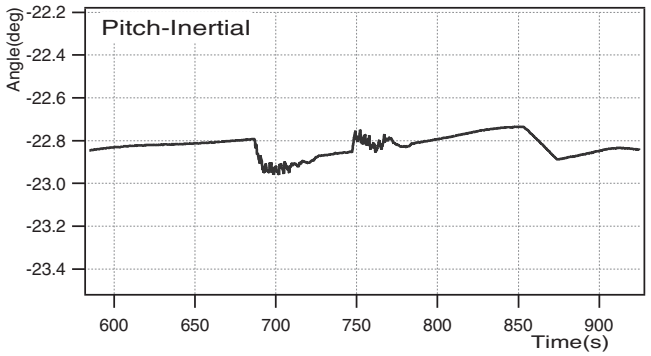

(b)

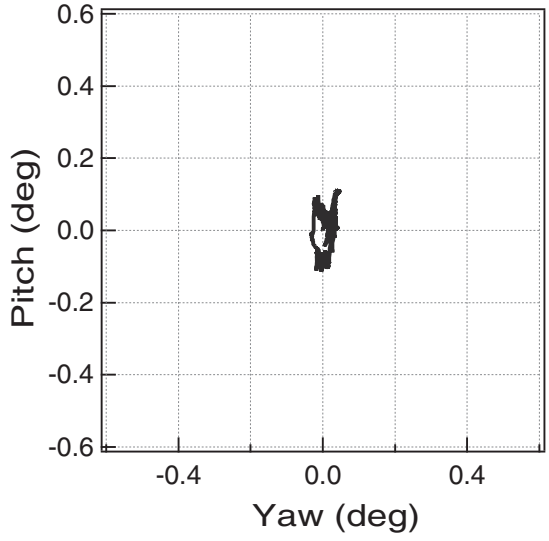

(c)

Fig. 8. Flight data for the experiment of the GJM-based inertial manipulation without attitude control: (a) spacecraft attitude (pitch); (b) hand orientation (pitch); (c) hand orientation error in the yaw–pitch plane.

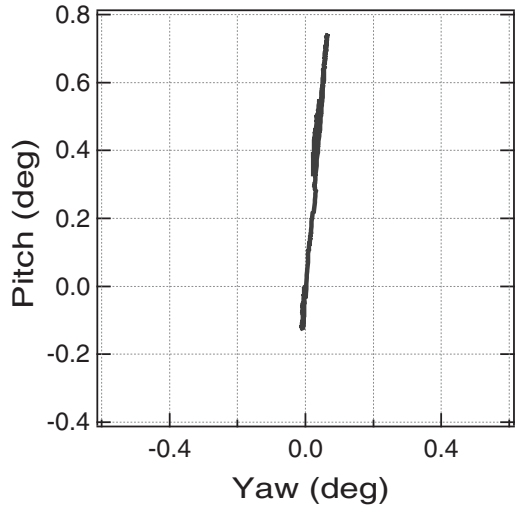

Fig. 9. Hand orientation error in the yaw–pitch plane in the experiment of the satellite-based manipulation with attitude control.

operated with respect to the satellite-based coordinate frame while the attitude of the base spacecraft is controlled by reaction wheels. With this control mode, the hand is also expected to accurately approach the target. Figure 9 shows a graph in the same format as Figure 8(c), for the manipulation of 200 mm at a velocity of 10 mm s^{-1} with respect to the satellite frame. In this case, however, the pitch error was greater than the previous case because the satellite's attitude fluctuates due to the reaction from the manipulator arm. After the manipulator motion ended, the error converged back to zero by means of the reaction wheels. However, the orientation error of the hand during the tracking was much greater than in the case with GJM and without the attitude control.

Here, it is clearly shown that the GJM-based inertial manipulation without base-attitude control is useful for both the target tracking and chasing operations. Moreover, it is certainly more advantageous than the conventional satellite-based manipulation strategy with base-attitude control, when measured in terms of error during the operation.

It should be noted that, in Figures 8(a) and (b), the attitude of the spacecraft slightly drifts (increasing in these cases) even when the manipulator arm does not make any motion. This drift is considered to be due to the gravity gradient torque. An analysis to this effect is made in Section 4.3.

4.2. RNS-Based Reactionless Manipulation

In the RNS experiment, several sets of reactionless trajectories were prepared based upon the RNS formulation. The trajectories were prepared either to go to or from useful control points, such as an on-board ORU or a target satellite. These trajectories were compared with the motion using conventional spline trajectories.

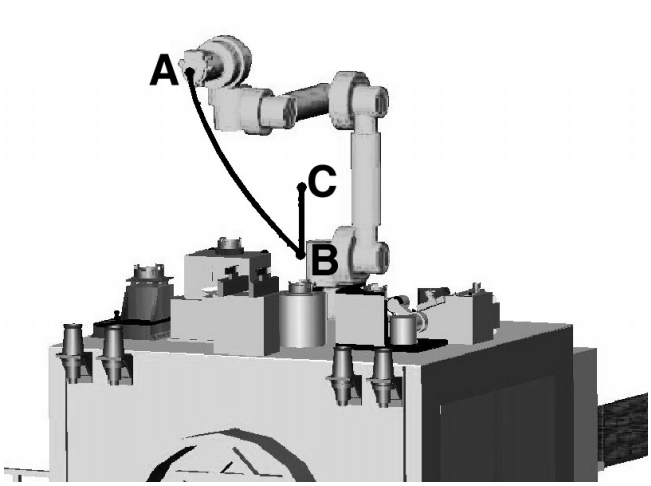

Fig. 10. Manipulator paths for the experiment of the RNS-based reactionless manipulation.

This experiment was carried out using reaction wheels to control the attitude of the base satellite. Even under the control, as was also shown in the previous experiment, the attitude disturbance was observed when the base received the manipulator reaction. This is because the control torque capacity of the reaction wheels is far smaller than the reaction torque from the arm. The attitude control provided by the reaction wheels mainly works for the recovery of the attitude after it was disturbed.

Figure 10 illustrates typical motion trajectories for this experiment. The path from points A to B is a conventional spline trajectory without the consideration for reactionless property. The path from B to C is a reactionless trajectory. The path from C back to B is again reactionless but different end-tip velocity was tested. Figure 11 depicts the corresponding flight data. The top graph shows the velocity norm of the manipulator hand, the middle graph shows the reaction momentum that was induced by the manipulation, and the bottom graph shows the attitude motion. During conventional spline manipulation, the motion from A to B, a relatively large momentum and attitude disturbance was generated. However, the RNS-based reactionless manipulation, the motion from B to C and C to B, yields very small reactions and disturbances. This comparison is very similar to the results obtained on the laboratory test bed shown in Figure 4.

In addition, it should be noted that for the reactionless manipulation, not only was the maximum attitude change remarkably small, but also the recovery time of the system. In practice, this recovery waiting time using the conventional manipulation is not negligible, and it degrades the efficiency of the operation. The reactionless manipulation, however, generates almost zero attitude disturbance and recovery time, thus assuring a very high operational efficiency.

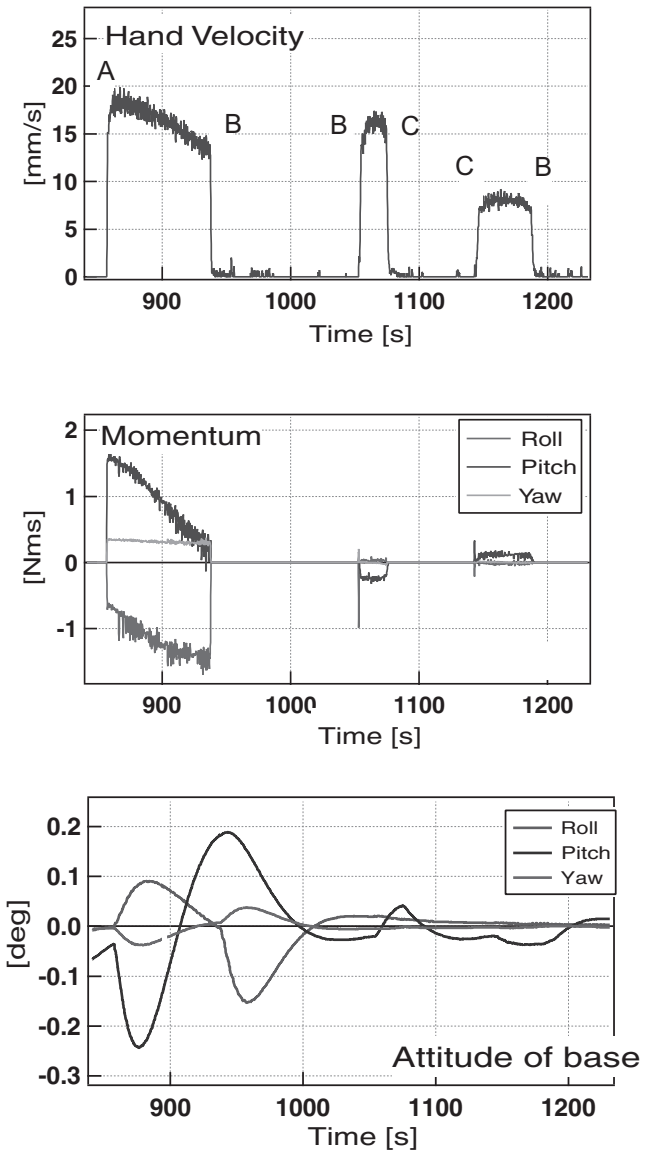

Fig. 11. Flight data for the experiment of the RNS-based reactionless manipulation.

4.3. Effect of Gravity Gradient Torque

Here the effect of the gravity gradient torque is briefly mentioned. In previous studies, it has been generally assumed that there are no external forces or moments on the control of a free-flying/floating space robot and, therefore, the total momentum of the system is conserved. However, in these experiments drift was observed both in the spacecraft's attitude in the case of no attitude control, and in the momentum of the reaction wheels in the case with attitude control. These examples suggest that an external moment is exerted on the spacecraft, and the source of these moments is believed to be the gravity gradient.

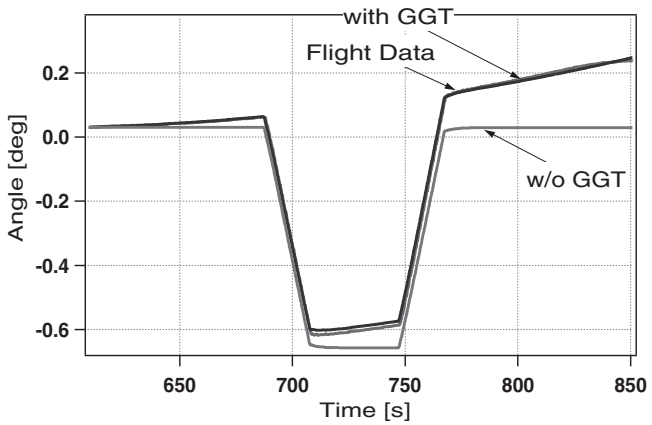

Fig. 12. Evaluation of the effect of the gravity gradient torque.

Figure 8(a) is revisited as Figure 12 in order to verify the effect of the gravity gradient torque. Using the flight data of the joint motion profile as input, the attitude motion of the spacecraft is simulated. With the assumption of zero external moments, the simulated attitude motion differs from the flight data (indicated as "w/o GGT"). However, when the gravity gradient torque is accounted for using eq. (10), the simulated result matches precisely with the flight data (indicated as "with GGT").

In case of the ETS-VII, which flies at an altitude of 550 km in low Earth orbit, the drift exceeds more than 1 degree for several minutes when the attitude control is turned off, due to the effect of the gravity gradient torque. If the spacecraft's antenna pointing error exceeds 1 degree, it may lose its high-bandwidth communication link. If this occurs, the link has to switch to a less capable, low-bandwidth communication mode. Therefore, in actual missions, free-drift operation should be limited to particular occasions, such as the final moment in the approach to a free-floating target. It is important to note, however, that the gravity gradient effect for a space robot becomes negligible when the altitude is increased to the geo-stationary orbit of 36 000 km.

5. Toward Practical Satellite Servicing

Various key technologies that could be potentially useful for future satellite servicing missions have been tested and demonstrated on the ETS-VII. In this section, these technologies are briefly reviewed from the point of view of the target capture operation.

Precise proximity flight controls are necessary when performing maneuvers in the approach of an end-of-life or malfunctioning satellite in orbit. In the ETS-VII mission, a 500 kg subsatellite was separated from the main body and was employed as a simulated target satellite.[2] The main part of the satellite then performed as a chaser. Three different approaching paths, called FP-1, 2 and 6, were tested. FP-1 and 2 took v-bar approach for rendezvous and FP-6 did r-bar approach. In these rendezvous experiments, autonomous sensor-based approach, precise proximity flight, and contingency maneuvers were demonstrated. All three paths resulted in a safe, autonomous soft-docking (Kawano et al. 1998).

In the case of a target capture, instead of a docking, the manipulator arm should track and grasp a fixture mounted on the target satellite while maintaining its proximity to the target. One of the current key technologies is visual servo-tracking of the grasping point. This was also successfully tested using on-board real-time video signal processing with a set of CCD cameras mounted on the manipulator hand and an optical marker located at the target fixture (Yoshida et al. 2000b).

Additional control technologies were verified. The purpose of these technologies is to improve the performance of the manipulator arm's final approach, thereby increasing the fidelity and the safe margin of a successful capture. As discussed earlier in this paper, these technologies are the GJM-based inertial manipulation and the RNS-based reactionless manipulation.

The goal of the reactionless manipulation is to operate the manipulator arm while not disturbing the attitude of the base satellite. Such manipulator trajectories are relatively limited in case of a 6-DOF arm, although they have been proven effective in minimizing the base attitude disturbance and the waiting time for attitude recovery. The RNS-based reactionless manipulation should be useful during the coarse approach to the target when the target is within the reach of the manipulator arm. In this situation, any attitude disturbance is highly undesirable.

The flight data show that the attitude fluctuated in the range of 0.5 degrees peak-to-peak during the nominal manipulator operation, which was conducted without the utilization of the reactionless manipulator trajectories. Although these fluctuations appear to be a small number, they are significant when measuring a spacecraft's attitude. For example, the attitude pointing accuracy is required in the order of 0.1 degrees, or even 0.01 degrees, in current spacecraft. In the case of the ETS-VII, the spacecraft was relatively robust so that an attitude error of more than 1 degree would cause the high gain antenna to lose its connection with the data-relay satellite, which could cause a suspension in the mission. However, the requirement on the attitude variation in a proximity flight is more serious. In the FP-2 operation, the ETS-VII experienced an unexpected attitude fluctuation during the final rendezvous approach to the target.[3] The spacecraft then immediately went

2. The target equips a radio transponder, optical reflectors, and a dedicated fixture. The target's attitude was stabilized. In this sense, the ETS-VII's subsatellite was the so-called *cooperative target.*

3. The reason of the attitude fluctuation was unstable behavior in one of the gas jet thrusters.

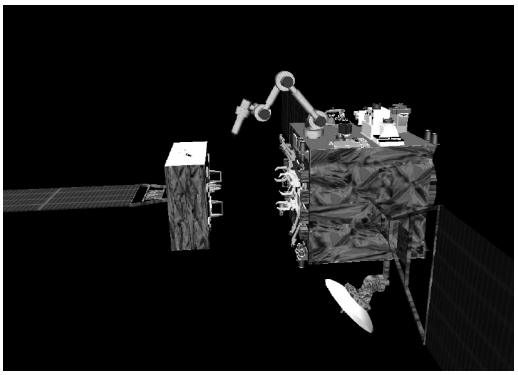

Fig. 13. A computer graphic image for the target capture simulation.

into a *safe-mode* and had to move back to the initial stage of the sequence, in which the chaser was located afar with a safe distance from the target.

When using visual servoing during the final approach, the control of the manipulator hand must be appropriate for a floating target in the inertial frame. In this phase, the GJM-based inertial manipulation, which proved effective in previous experiments, should be particularly useful. As discussed in this paper, the GJM manipulation without attitude control performs better than the satellite-based conventional manipulation with attitude control, when measured in terms of the orientation error in the hand positioning.

For satellite capture operations expected in the near future, a strategy can be developed that should yield the best combination of technologies. When the target enters within the limits of the manipulator arm's reach, the coarse approach using the RNS-based reactionless manipulation with attitude control is performed during the proximity flight of the spacecraft. In the fine approach, when the hand reaches within the final hundred millimeters to the grasping point, the control is switched to the GJM-based inertial manipulation with visual servo-tracking, and the spacecraft's attitude control is turned off.

Post-flight computer simulations are conducted in order to verify the advantage of using the combination of RNS and GJM concepts during a target capture operation. Figure 13 shows a computer graphic image illustrating the simulation's setup. The goal of the operation is to capture a freely floating target that is slightly drifting in the vicinity of the chaser. The specifications of the hardware and the performance of the servo-controllers are assumed to be the same as in the ETS-VII.

Now, the two-phase approach of the manipulator hand is tested. The hand is initially located about 400 mm from the fixture. During the coarse manipulation phase, the target is approached using the RNS-based reactionless manipulation, in such a way that the target fixture could be seen from the

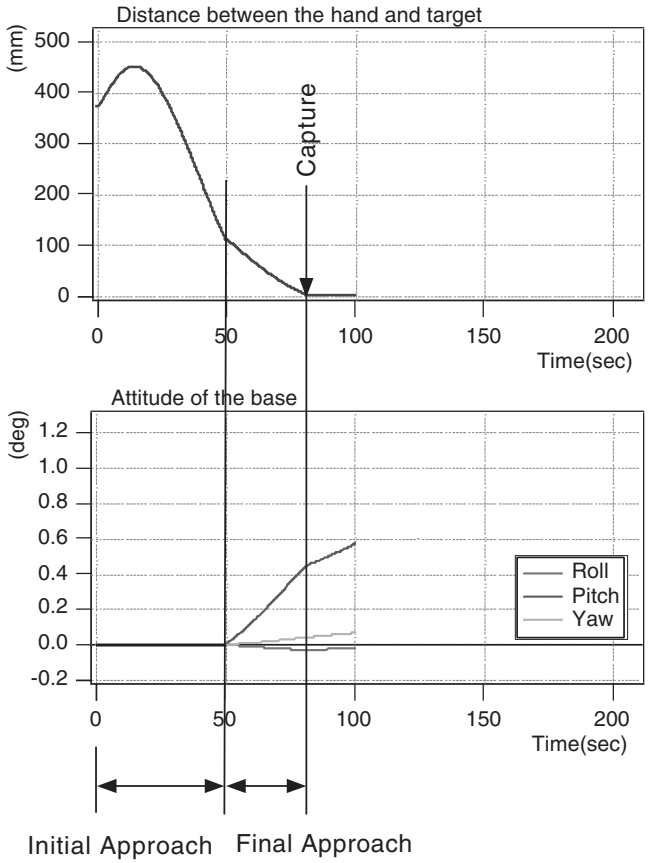

Fig. 14. Simulation for the autonomous target capture, case 1: RNS-based reactionless approach plus GJM-based inertial manipulation.

hand camera. When the hand error is less than 100 mm, the control is immediately switched to the GJM-based inertial manipulation with visual servo-tracking, and the spacecraft's attitude control is turned off.

Figure 14 depicts the distance between the hand and the target, and the attitude of the spacecraft during the simulation. Although the target was assumed to be drifting with a velocity of 10 mm s^{-1}, the two-phase manipulation performed smoothly. The attitude variation of the spacecraft was within 0.5 degrees from the turn-off of the attitude control to the capture. The motion picture of this simulation can be seen in Extension 4.

A counter example is shown in Figure 15. For this case, the given condition was exactly the same as the previous one. The differences for this case include (1) a conventional spline manipulation, instead of the RNS-based manipulation during the initial approach and (2) a conventional satellite-based manipulation, instead of the GJM-based manipulation during the final approach. The difference in the results is obvious. The latter case takes more than twice the amount of time to capture

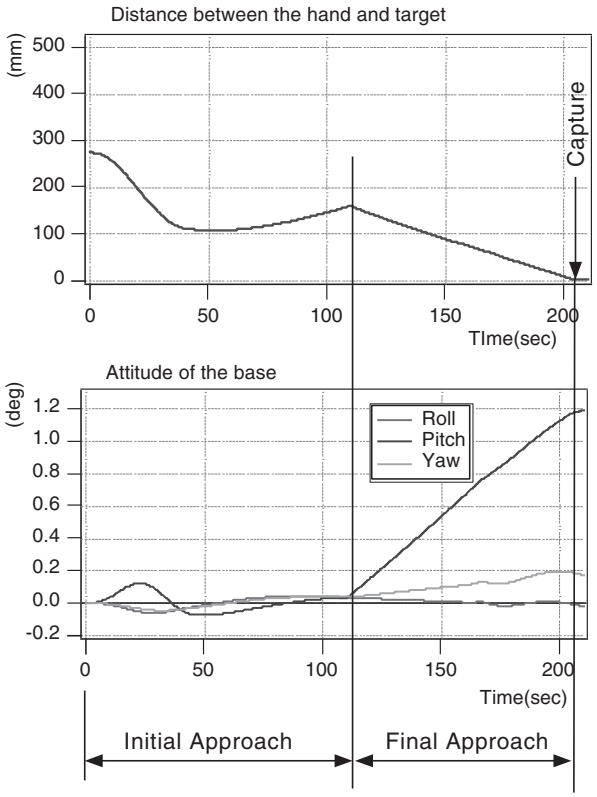

Fig. 15. Simulation for the autonomous target capture, case 2: conventional spline approach plus conventional satellite-based manipulation.

the target, disturbing the base spacecraft's attitude more than 1 degree. Also, the capture point was close to the boundary of the manipulator's reach. At such a configuration, the operation could be likely to fail because of reduced performance of the arm.

6. Conclusions

This paper presents the development and experimental verification of the space robot dynamics and control technology. The GJM-based inertial manipulation and the RNS-based reactionless manipulation have been theoretically studied since the mid-1980s, and their preliminary verifications have been conducted using simplified and confined laboratory test beds. Finally, these theories were verified through the demonstration of a real space robot in orbit.

Both the GJM-based and RNS-based control concepts were successfully verified on the ETS-VII. Other technologies that are relevant to the target capture, such as rendezvous control and visual servo-tracking of the manipulator hand, were also verified. The performance of the GJM-based manipulation reaching a given point in the inertial frame was validated by the flight data. The performance of the RNS-based reactionless manipulation was also substantiated with almost zero attitude disturbance and zero recovery time, thus assuring a high operational efficiency.

The effect of the gravity gradient torques, observed as the attitude drift of the satellite, was also addressed in the paper.

Computer simulations have demonstrated a promising control sequence for the autonomous capture of an object in space, which could prove useful in future orbital missions. Even though a different space robot will conduct the future missions, the same hardware specification as the ETS-VII was assumed as a reference system in the computer simulations. It was shown that a two-phase control sequence, including an RNS-based reactionless manipulation for the initial approach and a GJM-based inertial manipulation for the final approach, provided the most promising result for future missions.

Appendix: Index to Multimedia Extensions

The multimedia extension page is found at http://www.ijrr.org.

Table of Multimedia Extensions

Extension	Type	Description
1	Video	Target capture experiments carried out with a horizontal free-floating test bed, EFFORTS (1987, at Tokyo Institute of Technology). There are two elements: the first is the experiment to reach a static target which corresponds to Fig. 2(b); and the second is the experiment to chase a moving target with visual servo using a ceiling camera.
2	Video	Demonstration of the conventional manipulation and the reactionless manipulation using a test bed for flexible-base manipulator, TREP (1996, Tohoku University). Experiment 1 corresponds to Fig. 4(a). Experiment 2 corresponds to Fig. 4(b).
3	Video	Operation of the ETS-VII. Two different views of on-board cameras, a ground track of the orbit, and real-time simulation (1999, NASDA). The top right image corresponds to Fig. 6.
4	Video	Simulation of target capture operation by a combination of the RNS-based reactionless manipulation for the initial approach and the GJM-based inertial manipulation for the final approach. The motion corresponds to Fig. 14.

Acknowledgments

The author extends his special thanks to Dr Mitsushige Oda, Mr Noriyasu Inaba and other ETS-VII operation team members of NASDA, Japan, for their kind help and assistance in the preparation and execution of the collaborative flight experiments. The flight data of the ETS-VII were obtained through the collaboration of Tohoku University and NASDA.

References

Akin, D., and Howard, R. 1991. Neutral buoyancy simulation of space telerobotics operations. *Cooperative Intelligent Robotics in Space II, Proceedings of the SPIE* 1612:414–420.

Akin, D. L., Minsky, M. L., Thiel, E. D., and Curtzman, C. R. 1983. Space applications of automation, robotics and machine intelligence systems (ARAMIS) phase II. *NASA-CR-3734–3736*.

Alder, L., and Rock, S. 1994. Experiments in control of a flexible-link robotic manipulator with unknown payload dynamics: an adaptive approach. *International Journal of Robotics Research* 13(6):481–495.

Alexander, H., and Cannon Jr, R. 1987. Experiments on the control of a satellite manipulator. In *Proceedings of the TEEE American Control Conference*.

Dubowsky, S., and Torres, M. 1990. Minimizing attitude control fuel in space manipulator systems. In *Proceedings of the International Symposium on AI, Robotics and Automation (i-SAIRAS),* pp. 259–262.

Dubowsky, S., and Torres, M. 1991. Path planning for space manipulators to minimize spacecraft attitude disturbances. In *Proceedings of the IEEE International Conference on Robotics and Automation,* April, Sacramento, CA, Vol. 3, pp. 2522–2528.

Dubowsky, S., et al. 1994. A laboratory test bed for space robotics: the VES II. In *Proceedings of the IEEE/RSJ International Symposium on Intelligent Robot Systems (IROS'94),* Munich, Germany, pp. 1562–1569.

Fujii, H., Yoneyama, H., and Uchiyama, K. 1993. Experiments on cooperative motion of a space robot. In *Proceedings of the IEEE/RSJ International Conference on Intelligent Robots and Systems,* Tokyo, Japan, pp. 2155–2162.

Hirzinger, G., Brunner, B., Dietrich, J., and Heindl, J. 1993. Sensor-based space robotic-ROTEX and its telerobotic features. *IEEE Transactions on Robotics and Automation* 9(5):649–663.

Hughes, P. C. 1986. *Spacecraft Attitude Dynamics and Control*, Wiley, New York, Chapter 8, pp. 232–248.

Kasai, T., Oda, M., and Suzuki, T. 1999. Results of the ETS-7 mission—rendezvous docking and space robotics experiments. In *Proceedings of the 5th International Symposium on AI, Robotics and Automation in Space, iSAIRAS'99,* June 1999, ESTEC, the Netherlands, pp. 299–306.

Kawano, I., et al. 1998. First result of autonomous rendezvous docking experiments on NASDA's ETS-VII satellite. In *Proceedings of 49th International Astronautical Congress, IAF-98-A3.09*.

Koningstein, R., Ullman, M., and Cannon Jr, R. 1989. Computed torque control of a free-flying coorperating-arm robot. In *Proceedings of NASA Conference on Space Telerobotics,* Pasadena, CA, Vol. 5, pp. 235–243.

Mavroidis, C., Rowe, P. S., and Dubowsky, S. 1995. Inferred endpoint control of long reach manipulators. In *Proceedings of the International Conference on Intelligent Robots and Systems (IROS 95),* Pittsburgh, PA, pp. 71–76.

Mavroidis, C., Dubowsky, S., and Thomas, K. 1996. Optimal sensor location in motion control of flexibly supported long reach manipulators. In *Proceedings of ASME Design Technical Conference,* Irvine, CA, Paper No 96-DETC/MECH-1142.

Morimoto, H., Satoh, N., Wakabayashi, Y., Hayashi, M., and Aiko, Y. 2002. Performance of Japanese robotic arms of the international space station. In *15th IFAC World Congress*.

Nakamura, Y., and Mukherjee, R. 1991. Nonholonomic path planning of space robots via a bidirectional approach. *IEEE Transactions on Robotics and Automation* 7(4):500–514.

Nenchev, D. N., Yoshida, K., Vichitkulsawat, P., Konno, A., and Uchiyama, M. 1997. Experiments on reaction null-space based decoupled control of a flexible structure mounted manipulator systems. In *Proceedings of the IEEE International Conference on Robotics and Automation,* pp. 2528–2534.

Nenchev, D. N., Yoshida, K., Vichitkulsawat, P., and Uchiyama, M. 1999. Reaction null-space control of flexible structure mounted manipulator systems. *IEEE Transactions on Robotics and Automation* 15(6):1011–1023.

Oda, M. 1996. Coordinated control of spacecraft attitude and its manipulator. In *Proceedings of the IEEE International Conference on Robotics and Automation,* pp. 732–738.

Oda, M., et al. 1996. ETS-VII, space robot in-orbit experiment satellite. In *Proceedings of the IEEE International Conference on Robotics and Automation*, pp. 739–744.

Ohkami, Y., and Oda, M. 1999. NASDA's activities in space robotics. In *Proceedings of the 5th International Symposium on AI, Robotics and Automation in Space, iSAIRAS'99*, June 1999, ESTEC, the Netherlands, pp. 11–18.

Rui, C., Kolmanovsky, I., and McClamroch, N. H. 1998. Three-dimensional attitude and shape control of spacecraft with appendages and reaction wheels. In *Proceedings of the 32nd IEEE Conference on Decision and Control*, pp. 4176–4181.

Shimoji, H., et al. 1989. Simulation system for a space robot using 6 axis servos. In *Proceedings of the 11th IFAC Symposium on Automatic Control in Aerospace,* Tsukuba, Japan, pp. 131–136.

Umetani, Y., and Yoshida, K. 1987. Continuous path control of

space manipulators mounted on OMV. *Acta Astronautica* 15(12):981–986 (presented at the 37th IAF Conference, October, 1986).

Umetani, Y., and Yoshida, K. 1989a. Resolved motion rate control of space manipulators with generalized Jacobian matrix. *IEEE Transactions on Robotics and Automation* 5(3):303–314.

Umetani, Y., and Yoshida, K. 1989b. Experimental study on two-dimensional free-flying robot satellite model. In *Proceedings of NASA Conference on Space Telerobotics,* Vol. 5, pp. 215–224.

Vafa, Z., and Dubowsky, S. 1987. On the dynamics of manipulators in space using the virtual manipulator approach. In *Proceedings of the IEEE International Conference on Robotics and Automation,* pp. 579–585.

Vafa, Z., and Dubowsky, S. 1990. On the dynamics of space manipulators using the virtual manipulator, with applications to path planning. *Journal of Astronautical Sciences* 38(4):441–472.

Wargner-Bertak, C., Middleton, J., and Hunter, J. 1980. Shuttle remote manipulator system hardware test facility. *NASA-CP-2150,* pp.79–93.

Xu, Y., and Kanade, T. eds. 1993. *Space Robotics: Dynamics and Control*, Kluwer Academic, Dordrecht.

Yoshida, K. 1994. Practical coordination control between satellite attitude and manipulator reaction dynamics based on computed momentum concept. In *Proceedings of the IEEE/RSJ International Conference on Intelligent Robots and Systems,* Munich, Germany, pp. 1578–1585.

Yoshida, K. 1995. Experimental study on the dynamics and control of a space robot with the experimental free-floating robot satellite (EFFORTS) simulators. *Advanced Robotics* 9(6):583–602.

Yoshida, K. 1999. Space robot dynamics and control: To orbit, from orbit, and future. In *Robotics Research, The 9th International Symposium*, J. Hollerbach and D. Koditschek, eds, Springer, Berlin, pp. 449–456.

Yoshida, K., Nenchev, D. N., and Uchiyama, M. 1996. Moving base robotics and reaction management control. In *Robotics Research: The 7th International Symposium*, G. Giralt and G. Hirzinger, eds, Springer-Verlag, Berlin, pp. 101–109.

Yoshida, K., Nenchev, D. N., Vichitkulsawat, P., Kobayashi, H., and Uchiyama, M. 1997. Experiments on the point-to-point operations of a flexible structure mounted manipulator system. *Advanced Robotics* 11(4):397–412.

Yoshida, K., Nenchev, D. N., Inaba, N., and Oda, M. 2000a. Extended ETS-VII experiments for space robot dynamics and attitude disturbance control. In *22nd International Symposium on Space Technology and Science,* 25–29 May, Morioka, Japan, ISTS2000-d-29.

Yoshida, K., Hashizume, K., Nenchev, D. N., Inaba, N., and Oda, M. 2000b. Control of a space manipulator for autonomous target capture—ETS-VII flight experiments and analysis. In *AIAA Guidance, Navigation, and Control Conference,* 14–17 August, Denver, CO, AIAA2000-4376.

Yoshida, K., and Abiko, S. 2002. Inertia parameter identification of a space free-flying robot. In *AIAA Guidance, Navigation and Control Conference,* August, AIAA-2002-4568.